JOURNAL OF THEORETICAL AND APPLIED MECHANICS
48, 3, pp. 659-676, Warsaw 2010

ANALYSIS OF MAGNETIC FIELD EFFECT ON FERROMAGNETIC SPHERES EMBEDDED IN ELASTOMER PATTERN

Anna Boczkowska

Warsaw University of Technology, Faculty of Materials Science and Engineering, Warsaw, Poland
e-mail: abocz@meil.pw.edu.pl

Leszek Czechowski, Mieczysław Jaroniek

Technical University of Lodz, Faculty of Mechanical Engineering, Łódź, Poland
e-mail: lczechow@p.lodz.pl; mieczyslaw.jaroniek@p.lodz.pl

Tadeusz Niezgoda

Military University of Technology, Faculty of Mechanical Engineering, Warsaw, Poland
e-mail: t.niezgoda@wat.edu.pl

The results of modelling of the magnetorheological elastomers (MREs) microstructure using Finite Elements Method (FEM) are shown. MREs are solids analogous to magnetorheological fluids consisting of carbonyl-iron particles and a soft elastomer matrix. Fabrication of MREs is performed in an external constant magnetic field. Due to the presence of this field, the ferromagnetic particles tend to arrange themselves into elongated chains according to the magnetic field lines. FEM analysis of the MREs microstructure takes into account two cases: magnetic power and elastic vectors as well as their interactions between the components of the composite. The paper describes spatial ordering of the particles based on their interactions with the magnetic field. Two phenomena were taken into account: the force of a magnetic field and the local magnetic dipoles. Both fields have been modelled for a circular conductor with electrical current.

Key words: magnetorheological elastomers, Finite Element Method, photoelastic method

1. Problem formulation

Magnetorheological elastomers (MREs) are solid phase analogues of magnetorheological fluids. The MREs consist of ferromagnetic carbonyl-iron particles and a soft elastomer matrix. Their mechanical properties change because of

the influence of an external magnetic field (Dorfmann and Brigadnov, 2003; Lokander and Stenberg, 2003b, Zienkiewicz and Taylor, 1994). According to the literature, the elasticity modulus of MREs can undergo a change by about 30-40%, and even 60% (Dorfmann and Brigadnov, 2003; Kankanala and Trianta fyllidis, 2004) due to the presence of the magnetic field.

MREs most often consist of iron micro-dimensional particles, although in the literature we can find examples of application of various particles from carbonyl-iron and iron alloys (Lokander *et al.*, 2004) to magnetostrictive particles (Lokander and Stenberg, 2003a). Size and shape of the particles applied in MREs can be different (Farshad and Benine, 2004; de Vicente *et al.*, 2002).

A huge interest in MRE application to technology causes the necessity of their theoretical description (Connoly and McHugh, 1999). A significant obstacle to publish materials concerning MREs and their properties is the lack of description of magneto-elastic deformation. Some solutions on the basis of Cauchy's elastic theory for isotropic magnetic sensitive bodies were found (Jolly *et al.*, 1999).

These theoretical results are not always agreeable with experimental results. In literature, one can find a lot of mathematical models describing deformation of MREs under the influence of a magnetic field (Dorfmann and Brigadnov, 2003; Dorfmann and Ogden, 2003; Dorfmann *et al.*, 2004). Some of them even assume that there is various magnetization in the range of ferromagnetic particles (Bocera and Bruno, 2001). This phenomenon does not occur for appropriately small particles of dimensions $\leqslant 1.5\,\mu$m. In the case of greater particles, this effect has to be taken into consideration in mathematical equations, what is described in Bocera and Bruno (2001).

Other models are focused on analysis of a limited number of particles which are within limits of the same radius (Yin *et al.*, 2002). Constitutive equations for composites consisting of magnetic particles in an elastomer matrix and subjected to deformations can be described according to Eshelby's approximation.

A combination of the finite element method with the "meshfree" method, makes possible creation of a discrete model subjected to one-axial deformation with or without the presence of a magnetic field (Kleiber, 1985). FEM description can be found in many works (Kleiber, 1985; Lokander ans Stenberg, 2003a,b; Lokander *et al.*, 2004; Turner *et al.*, 1956; Wang *et al.*, 2003; Woźniak, 1993, 1995; Yin *et al.*, 2002; Zhou, 2003; Zienkiewicz and Taylor, 1994). FEM is based on the assumption that a solid might be considered as a collection of finite elements connected to each other with the use of finite nodal points.

The FEM concept introduced by Turner *et al.* (1956) and Zienkiewicz and Taylor (1994) assumes finite elements which are bounded by a number of nodal points. FEM enables analysis of objects with complex geometry and can be applied for a material model in a combined internal structure (Wang *et al.*, 2003; Zienkiewicz and Taylor, 1994) provided that a proper model can be created and its division into finite elements can be carried out.

Many works, related to some extent with the subject of this paper were devoted to analysis of the magnetic field using the finite element method as well. Only few of them are described here in short. Matsui and Okuda (1998), for instance, proposed a scheme for calculating the magnetic field in a spherical shell, based on the Earth's outer core. According to their results, they suggested that the accuracy of the dipole field depends on the radius of the simulation domain. In Tomczyk and Koteras (2008), the authors presented results of an experimental and numerical study of the influence of the air gap between the coils in a transformer. They obtained a good agreement between both investigations. Broeh *et al.* (1996) showed results of the finite-element method in combination with the Biot-Savart law concerning the magnetic field distribution generated by a dipolar source within a homogeneous volume conductor of an arbitrary shape. Simulations were performed to evaluate the numerical accuracy for a homogeneous spherical volume conductor.

In this paper, the effect of the magnetic field on the elastomer pattern containing steel spheres is shown. The theoretical description of the influence of magnetic field lines on ferromagnetic particles and the determination of forces is rather complicated. The whole analytical calculations concerning the knowledge of attraction of the spheres are usually simplified by the assumption of one concentrated force acting in gravity centre of the body. Such an approach allows one to obtain only approximated results, however, the numerical model makes possible the determination of forces in each point of the discrete body. In this manner, the resultant forces can be found, which allows one to compute stresses and displacements in the elastomer pattern. The fundamental aim of the work was to determine the limit value of the magnetic field in order to destruct elastomer continuity. Two tests (numerical and empirical) were performed.

In the numerical model, the source of the magnetic field is a solenoid through which an electrical current passes. Numerical computations for the spatial model which consists of the solenoid generating the magnetic field and of the elastomer pattern with two spheres have been conducted. The elastomer pattern has no magnetic property and the source of appearing stresses in it is caused by displacements of the spheres due to the magnetic field. The problem

is solved by applying the finite element method in ANSYS 11.0 code. For given current values, results have been presented in forms of magnetic field intensity, magnetic induction, magnetic forces, stresses and displacements. The applied numerical method is particularly presented in the third Section.

In the experimental model, real elastomer patterns in which two spheres with diameter 12.7 mm had been set were prepared. The experimental approach allowed one to observe stress distribution in the material.

2. Material properties

The values of mechanical properties of the elastomer are found by performing a one-directional tensile test. In numerical modelling of the magnetic field, the effect of elastic deformation of spheres and elastomer is assumed (Table 1). Because of good cohesion of the spheres and elastomer material condition of deformation continuity at the border of two bodies has been assumed.

Table 1. Assumed material properties

Ferritical steel		Elastomer	
Young's modulus E [MPa]	Poisson's ratio ν [–]	Young's modulus E [MPa]	Poisson's ratio ν [–]
200000	0.3	0.12	0.45

3. Numerical model (ANSYS 11.0 code)

In the numerical model, a homogeneous magnetic field has been assumed. This was achieved by incorpolation of a solenoid, which generates a homogeneous magnetic field as a result of an electric current flowing through a wire. The assumption that inside a real solenoid the magnetic field is predominantly homogeneous is to some degree a simplification, although in numerical computations it is acceptable.

The current passing through a wire of a solenoid produces the magnetic field according to the relation

$$H = \frac{nI}{l} \tag{3.1}$$

where n is the number of coils (in the FEM model amounts 1), I [A] – current passing through one coil, l [m] – height of the solenoid.

The value of magnetic induction B is expressed by the equation as

$$B = \mu H \tag{3.2}$$

where $\mu = \mu_{air}\mu_0$ is the absolute magnetic permeability, $\mu_0 = 4\pi 10^{-7} H/m$ – magnetic permeability of vacuum, $\mu_{air} = 1$ – relative magnetic permeability of the air.

In Fig. 2, the elements type *source* are shown as the solenoid producing the magnetic field. Dimensions of the elastomer pattern and spheres are presented in Fig. 1.

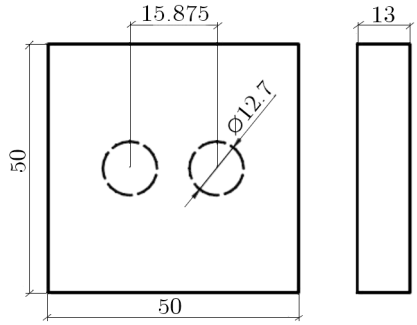

Fig. 1. Dimensions of the elastomer pattern and spheres, [mm]

In Fig. 2, the solenoid for modelling of the magnetic field is shown.

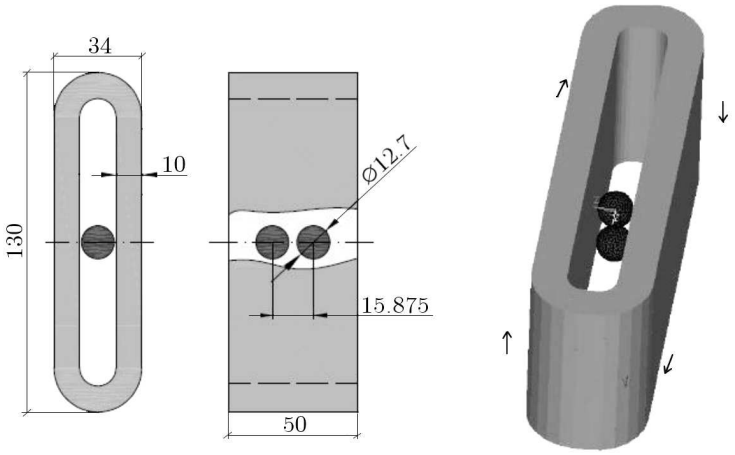

Fig. 2. (a) Dimensions of the solenoid and spheres (solenoid: length, width, height, thickness: 130 mm × 34 mm × 50 mm × 10 mm), (b) partially numerical model for computations in Ansys 11.0 code

The elastomer pattern of dimensions 50 mm × 50 mm × 13 mm with two steel spheres has been set inside the solenoid and the whole space around it is surrounded by the air (dimension of the air space amounts 100 mm × 100 mm × 200 mm). The relative magnetic permeability for steel spheres is assumed $\mu_{steel} = 10^4$, and for the elastomer pattern $\mu_{elastomer} = 1$. Numerical calculations have been carried out in two stages, namely: firstly, to find magnetic forces appearing only on spheres (it is assumed that the elastomer pattern has no magnetic property) and secondly, to determine the stress and displacement distribution for these forces. In numerical calculations, Biot-Savart's formula was used for finding the magnetic forces.

The three-dimensional numerical model has been divided into finite elements (for the spheres and elastomer pattern 13958 and 13608 elements, respectively). For investigation of the magnetic field, an element type *solid98* with six degrees of freedom at each node was applied. In order to determine stresses and displacements, an element type *solid92* was used. For the elastomer pattern, the following boundary condition has been assumed: displacement on two external surfaces is equal to zero in all directions (Fig. 3).

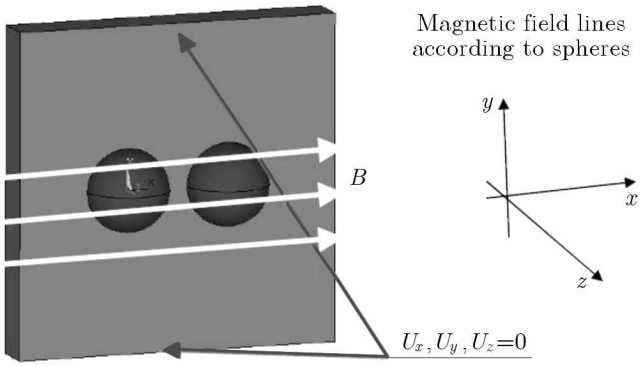

Fig. 3. Division into finite elements and assumed boundary conditions

4. Physical model of MRE (photoelastic model)

A physical model of a MRE is made of polyurethane polymer (PU) formed by synthesis of two polyols VORALUX® HF 505 and 14922 and Isocyanate HB 6013 compound, delivered by Dow Chemical Company. There is a composite model performed in an analogous way as the real MRE created at Warsaw University of Technology. Inside the elastomer pattern of dimensions 50 mm × 50 mm and thickness 10 mm, two low alloy steel spheres of diame-

ters 12.7 mm were placed. The distance between the gravity center of steel elements is 15.875 mm.

Elastomer PU is optically active what means that under the influence of the stress state appearing in it and in a polarized light it indicates birefringence. This property enables one to analyse the stress and strain state caused by the magnetic field using the photoelastic method.

4.1. Optical and mechanical properties of the elastomer

Photoelastic measurements enabled examinations of deformations and stresses in the whole structure of the elastomer. On the basis of photoelastic measurements, we can directly define the difference of stresses or main strains

$$\sigma_1 - \sigma_2 = k_\sigma m \qquad \varepsilon_1 - \varepsilon_2 = \frac{1+\nu}{E}(\sigma_1 - \sigma_2) = \frac{1+\nu}{E} k_\sigma m \tag{4.1}$$

where: $k_\sigma = (\sigma_1 - \sigma_2)/m$, $f_\varepsilon = k_\sigma(1+\nu)/E$ are model constants corresponding to the difference of stresses and main deformations.

The values of model constants corresponding respectively to the difference of main stresses k_σ or main strains f_ε on the basis of the compression test of a cuboid of dimensions 50 mm × 50 mm × 10 mm located in polariscope space have been determined. The results of the compression test are as in Table 2.

Table 2. Results of the compression test

Force P [N]	Thickness g [mm]	Width b [mm]	Stress $\sigma = P/(gb)$ [MPa]	Order of isochromatic m	Photoelastic constant $k = \sigma/m$ [MPa/is.ord.]*
9	10	50	0.018	1	0.018
26.5	10	50	0.053	3	0.018

* is.ord. – isochromatics order

The material characteristic and Young modulus obtained experimentally were assumed in the investigations.

Using the material characteristic and Young modulus found on the basis of compression tests performed in polariscope, the optical properties (model constants) of elastomer have been then determined.

As it is well known, the lines for which the differences between stresses and main strains have a constant value and the same color are called the isochromatics. Basing on isochromatics measurements, the stress distribution has

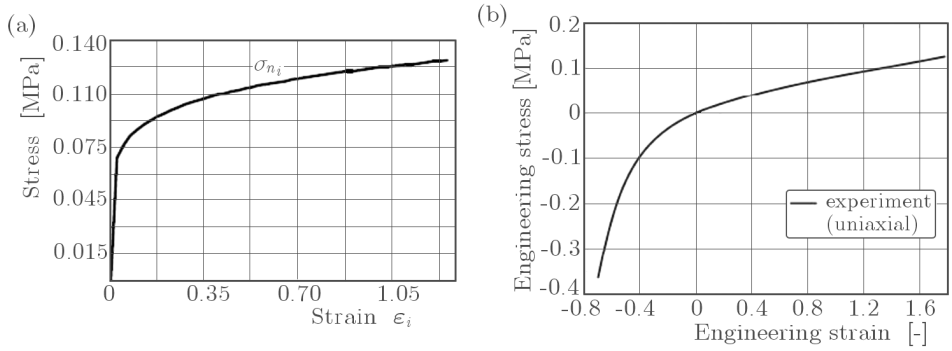

Fig. 4. Strain-stress curves for the pure elastomer pattern in the case of (a) tensile test, (b) tensile-compression test

been defined. Applying the stress-strain relation, in an elastic body deviator strain components are proportional to deviator stress components, as written

$$\frac{\sigma_1 - \sigma_{sr}}{\varepsilon_1 - \varepsilon_{sr}} = \frac{\sigma_2 - \sigma_{sr}}{\varepsilon_2 - \varepsilon_{sr}} \tag{4.2}$$

The result of photoelastic measurements can also be applied to strain and stress analysis concerning elastic-plastic materials. In an elastic-plastic body, the proportion of deviator strain components and deviator stress components is described by the relation

$$\frac{\sigma_1 - \sigma_{sr}}{\varepsilon_1 - \varepsilon_{sr}} = \frac{\sigma_2 - \sigma_{sr}}{\varepsilon_2 - \varepsilon_{sr}} = 2G' \qquad G' = \frac{\tau_0}{\gamma_0}\Big(\frac{\gamma}{\gamma_0}\Big)^{N-1} \tag{4.3}$$

where N is the hardening exponent, in the elastic-plastic body for $\gamma \geqslant \gamma_0$, $\tau = \tau_0(\gamma/\gamma_0)^N$, τ_0 and γ_0 are the yield stress and yield strain, and G' is secant shear modulus.

For a simple tensile test, when $\sigma_1 = \sigma$, $\sigma_2 = \sigma_3 = 0$, the parameters $\varepsilon_1 = \varepsilon_{int}$, ε_2 and ε_3 can be determined on the basis of the shape change law $\varepsilon_2 = \varepsilon_3 = -(\varepsilon_{int} - 3\varepsilon_{sr})/2$, where $\sigma_{int} = \sigma = A\varepsilon^P$ and $\varepsilon_{int} = (\sigma_{int}/A)^{1/p}$ or $\sigma_{sr} = \sigma/3$.

The main strain difference amounts

$$\varepsilon_1 - \varepsilon_2 = \frac{3}{2}\varepsilon_{int} - 3\varepsilon_{sr} \tag{4.4}$$

The model constant should be replaced with the function presenting the main strain difference in terms of isochromatics loops

$$\varepsilon_1 - \varepsilon_2 = f_\varepsilon(m)m \tag{4.5}$$

For the considered materials, the substituted Poisson's ratio ν_{s-pl} value ranges from 0.45 to 0.49. In the case of a disc loaded by focused force, well known formulas are used.

The model constant of the elastomer for the assumed characteristic amounts $k_\sigma = 0.0183\,\mathrm{MPa/(is.ord)}$.

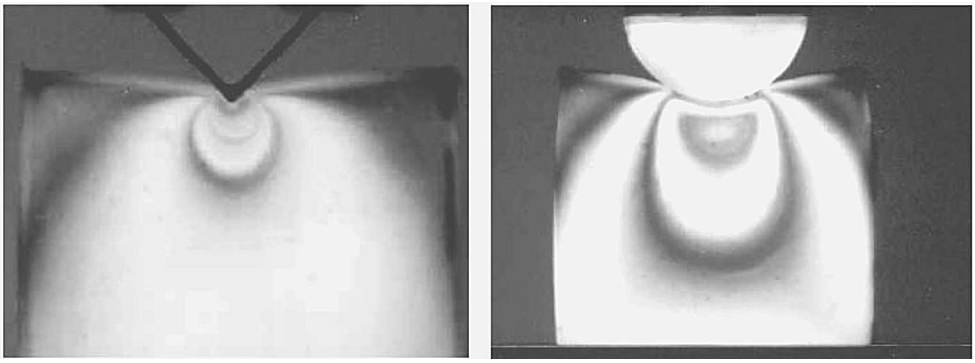

Fig. 5. Isochromatics distribution of the sample loaded by a focused force for great deformations shown on bright and dark photos

For the material with a nonlinear characteristic

$$\begin{aligned} &\sigma = \sigma_0\Big(\frac{\varepsilon}{\varepsilon_0}\Big)^p && E_s = \frac{\sigma_0}{(\varepsilon_0)^p}\varepsilon^{p-1} \\ &\sigma_\theta - \sigma_r = \frac{2P}{\pi g}\frac{(\cos n\theta)^p}{r} && n^2 = \frac{1-2\mu}{\mu^2} \\ &r = \frac{2P}{\pi g}\frac{(\cos\theta)^p}{\sigma_\theta - \sigma_r} \end{aligned} \tag{4.6}$$

The model constant of the elastomer for the nonlinear characteristic is

$$k_\sigma(m) = \frac{\sigma_0}{\varepsilon_0^p}\frac{\varepsilon^p}{m}\Big[1 - \frac{2}{3}(1-2\nu_0)\Big(\frac{\varepsilon}{\varepsilon_0}\Big)^{p-1}\Big] \qquad \sigma = \sigma_0\Big(\frac{\varepsilon}{\varepsilon_0}\Big)^p \tag{4.7}$$

where: $\sigma_0 = 0.0183\,\mathrm{MPa}$, $\varepsilon_0 = 0.1375$, $\nu_0 = 0.45$, $E_0 = 0.12\,\mathrm{MPa}$.

5. Results

5.1. Numerical investigation

Delivering a suitable magnetic field value that have an effect on the spheres was performed by a current flow passing through a coil wire. The numerical

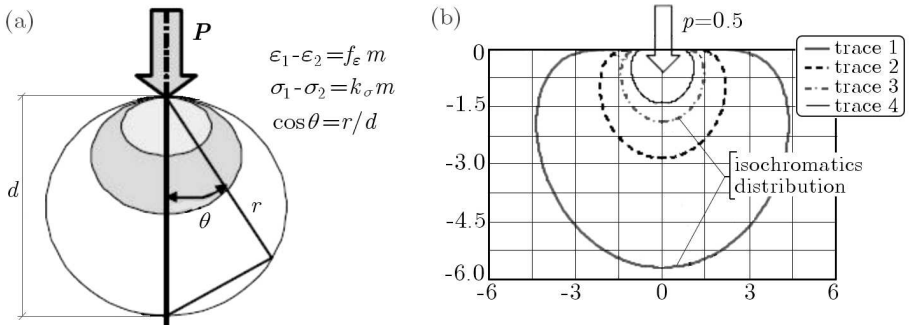

Fig. 6. Isochromatics distribution found on the basis of nonlinear characteristic of the sample loaded by focused force for great deformations

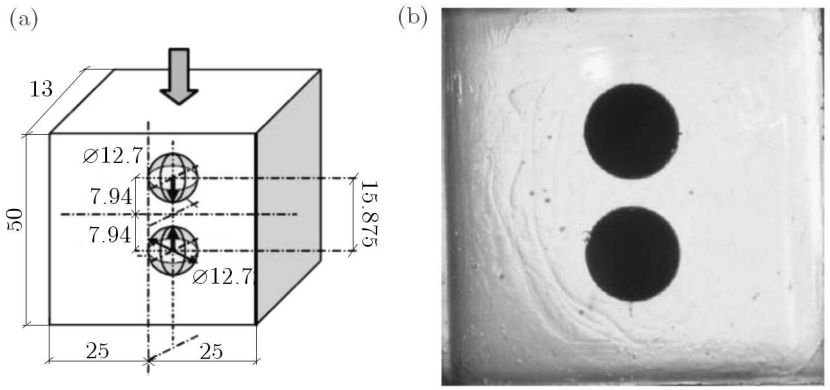

Fig. 7. Elastomer model used in the investigations: (a) dimensions, (b) model photo without load in polariscope in sodium light

model differs from the real one since there is one-coil solenoid, whereas in the numerical study this fact does not has a significant influence.

Numerical computations have been carried out for a various current flow values to determine the magnetic field influence on stresses in the elastomer pattern. The calculations were initiated at the current $I = 5 \cdot 10^3$ A and is further gradual increase until the spheres got in touch with each other. On the basis of theoretical relation (Eq. (3.2)), one can determine the desired magnetic induction inside the solenoid, assuming the conditions as in pure air. Hence, the current $I = 5 \cdot 10^3$ A flowing through this solenoid corresponds to magnetic induction 0.125 T.

Most of the obtained results has been shown in the middle plane (passing through the gravity centre of the spheres) in order to observe the part of the elastomer pattern between the spheres. In Fig. 8, a scalar magnetic field

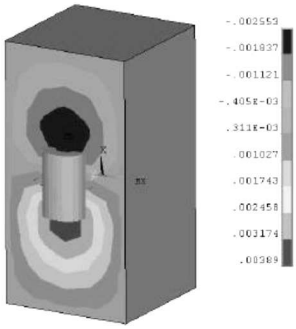

Fig. 8. Scalar magnetic field distribution for the whole numerical model [Vs/m^3]

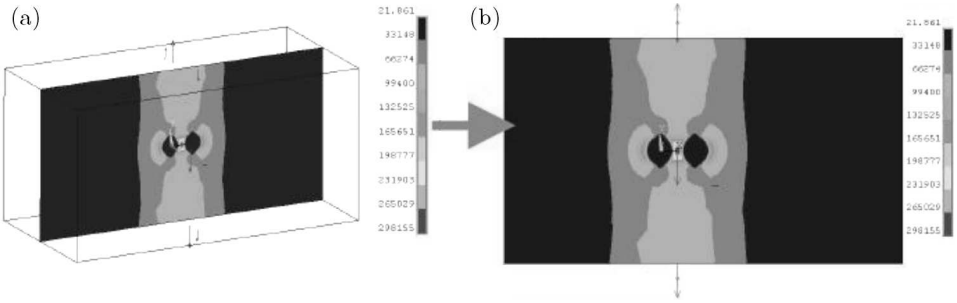

Fig. 9. Resultant magnetic field intensity H_{sum} [A/m] for the plane passing through the gravity centre of the spheres

distribution for the whole numerical model is shown. In Figs. 9a,b, the resultant magnetic field is presented. Between the spheres, the greatest intensity of magnetic field amounting to 300000 A/m was noticed. On the other hand, in Figs. 10a,b, the magnetic induction distribution, where the limited value reaches 0.44 T, is displayed.

The essential part of numerical calculations was to outline the magnetic forces. The resultant displacements and von Mises stress distribution have been calculated for the determined magnetic forces, what is presented in Figs. 11 and 12. The maximum resultant al summary displacement for any discrete element at magnetic induction 0.125 T was equal to about 0.11 mm. By these parameters, von Mises stress in the elastomer came to 0.011 MPa.

Repeating the above described calculation course for higher magnetic induction values, it was decided in the farther part of work to show only displacements and stresses in the elastomer pattern. The limiting current value flowing through the solenoid was assumed when the spheres contacted each other. On this basis, the diagram (Fig. 13) which shows the relation between the magne-

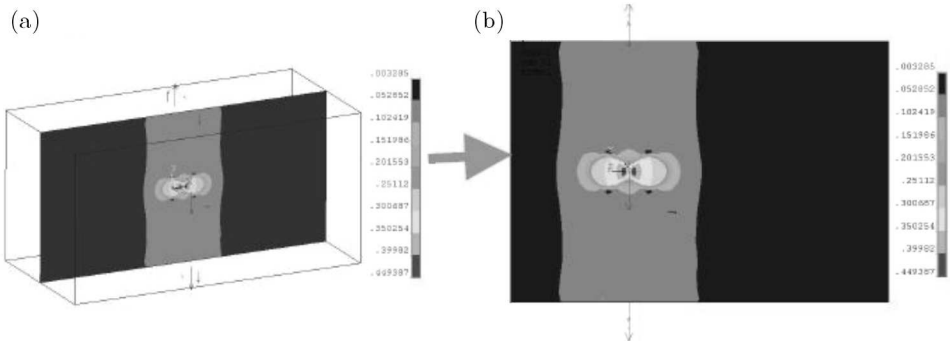

Fig. 10. Resultant magnetic induction B_{sum} [T] for the plane passing through the gravity centre of the spheres

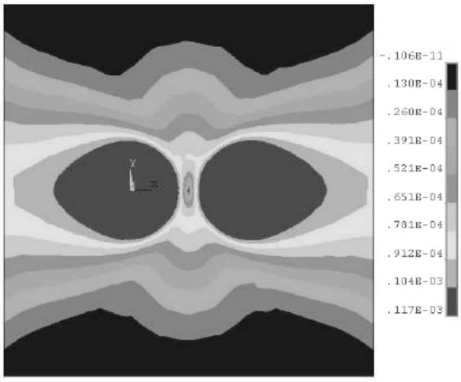

Fig. 11. Resultant displacement u_{sum} [m]

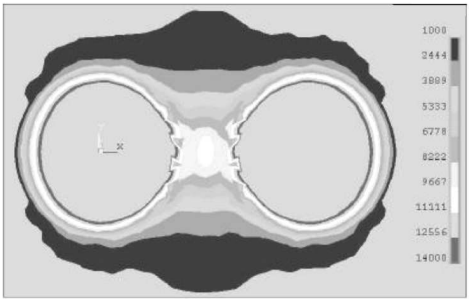

Fig. 12. Von Mises stress distribution σ_{red} [Pa]

tic induction and the maximum resultant displacement or maximum von Mises stress in the elastomer has been created. It can be stated that, theoretically, the contact of spheres occurs at the magnetic induction 0.44 T.

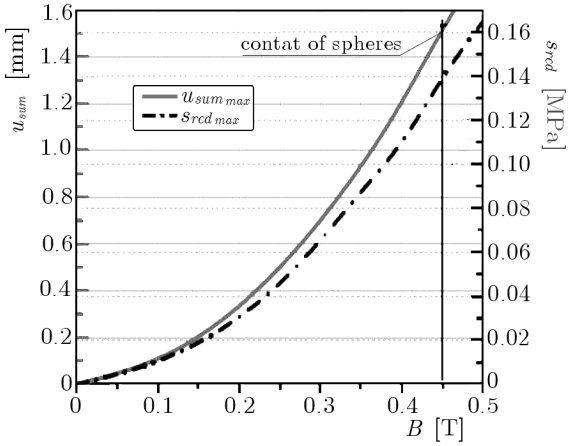

Fig. 13. Maximum displacements and von Mises stresses depending on magnetic induction for the spheres of diameter 12.7 mm

5.2. Experimental results

In Fig. 14, the vertical displacement distribution obtained by FEM in ANSYS 11.0 code as well as the result determined experimentally (Fig. 14b) on the surface of the real elastomer pattern are illustrated. The displacement distribution found in the empirical model, enables determination of stresses and deformation only on the external surface of the elastomer. However, the map in Fig. 14a presents displacements in the middle plane of the elastomer. The photoelastic study makes it possible to evaluate the average stresses in the plane of the model.

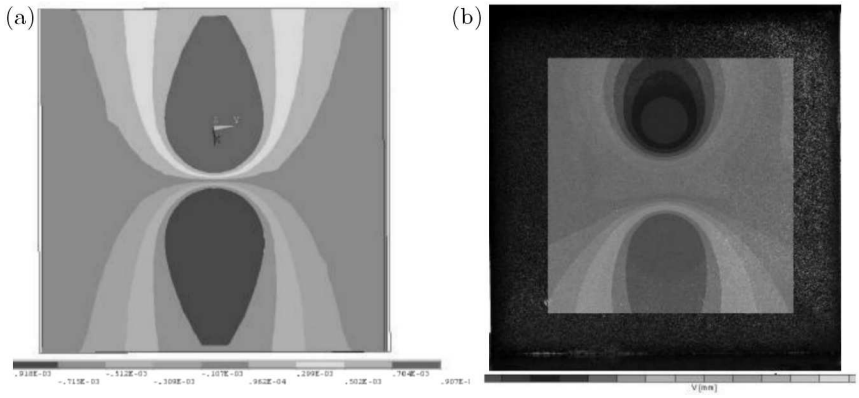

Fig. 14. Vertical displacement distribution [m]

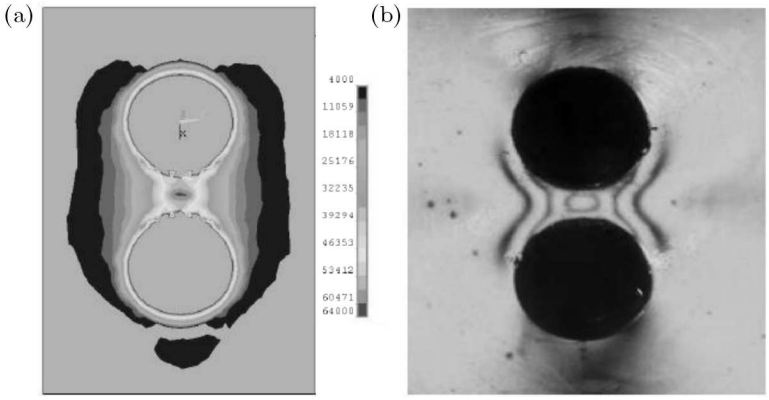

Fig. 15. Isochromatics between the spheres for magnetic induction 0.3 T: (a) $\sigma_1 - \sigma_2 = 0.064$ MPa (numerical model) and (b) $\sigma_1 - \sigma_2 = k_\sigma m = 0.063$ MPa (experimental model) for $k_\sigma = 0.0183$ MPa/is.ord., $m = 3.5$

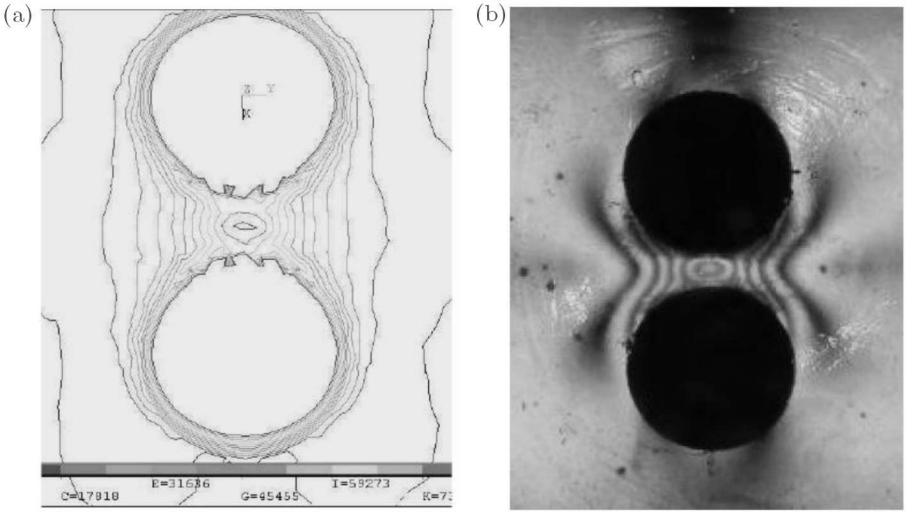

Fig. 16. Isochromatics between the spheres for magnetic induction 0.35 T: (a) $\sigma_1 - \sigma_2 = 0.088$ MPa (numerical model) and (b) $\sigma_1 - \sigma_2 = k_\sigma m = 0.091$ MPa (experimental model) for $k_\sigma = 0.0183$ MPa/is.ord., $m = 5$

6. Final conclusions

In the paper, numerical investigation results as well as experimental results of the effect of magnetic field on steel spheres embedded in an elastomer have been presented. In the numerical computation, an ANSYS 11.0 code was used

basing on the finite elements method. The obtained results have been shown in form of maps of physical magnitudes (magnetic field intensity, magnetic induction, displacements and stresses). In the experimental study, the knowledge about elasto-optics was applied. The source of real magnetic field generation was a two-pole electromagnet made by SEIKO company. After conducting the examinations, the following remarks can be stated:

- Distribution of the magnetic field intensity in pure air created by the solenoid in which there is a steel element, depends on the magnetic permeability and shape of the ferromagnetic body (see H and B distribution in Fig. 9 and Fig. 10).
- Complete contact of spheres under the influence of the magnetic field occurs at $0.44\,\mathrm{T}$ and the maximum effective stress according to the Mises formula was equal to $0.15\,\mathrm{MPa}$ (Fig. 14).
- In the numerical model, it can be assumed that in the space inside the solenoid filled with air, the magnetic field intensity is homogeneous and can be determined according to Eq. (3.1).
- Comparison between formulation of the numerical model (assumed boundary conditions, see Fig. 3) and the boundary condition in the real model is of no importance. The support for the real model has been also verified numerically.
- On the basis of the elastomer pattern model, the photo-elasticity constant was determined. Next, isochromatic distributions corresponding to the magnetic induction at $0\,\mathrm{T}$ - $0.35\,\mathrm{T}$ were set. A good enough accordance of the results obtained numerically and experimentally can be stated. In this case, the fact that both studies have a comparative character should be noticed. However, the suggested investigation method can be applied to numerical computations for a real MRE filled with carbonyl-iron particles of dimensions from several to over a dozen μm.

References

1. Banks H.T., Pinter G.A., Potter L.K., Gaitens M.J., Yanyo L.C., 1999, Modeling of nonlinear hysteresis in elastomer under uniaxial tension, *Journal of Intelligent Material Systems and Structures*, **10**
2. Bocera L., Bruno O., 2001, On the magneto-elastic properties of elastomer – ferromagnet composites, *Journal of the Mechanics and Physics of Solids*, **49**, 2877-2919

3. Broeh S.P., Zhou H., Peters M.J., 1996, Computation of neuromagnetic fields using finite-element method and Biot-Savart law, *Medical and Biological Engineering and Computing*, **34**

4. Connoly P., McHugh P.E., 1999, Fracture modeling of WC-Co hardmetals using crystal plasticity theory and the Gurson model, *Fatique and Fracture of Engineering Materials and Structures*, **22**

5. Dorfmann A., Brigadnov I.A., 2003, Mathematical modeling of magneto-sensitive elastomers, *International Journal of Solids and Structures*, **409**, 4659-4674

6. Dorfmann A., Brigadnov I.A., 2004, Constitutive modeling of magneto-sensitive Cauchy-elastic solids, *Computational Materials Science*, **29**, 270-282

7. Dorfmann A., Ogden R.W., 2003, Magnetoelastic modeling of elastomers, *European Journal of Mechanics A/Solids*, **22**, 497-507

8. Dorfmann A., Ogden R.W., Saccomandi G., 2004, Universal relations for non-linear magnetoelastic solids, *International Journal of Non-Linear Mechanics*, **39**, 1699-1708

9. Farshad M., Benine A., 2004, Magnetoactive elastomer composites, *Polymer Testing*, **23**, 347-353

10. Jolly M.R., Carlson J.D., Munoz B.C, Bullions T.A., 1996, The magnetoviscoelastic response of elastomer composite consisting of ferrous particles embedded in a polymer matrix, *Journal of Intelligent Material Systems and Structures*, **7**, 613-622

11. Kankanala S.V., Triantafyllidis N., 2004, On finitely strained magnetorheological elastomers, *Journal of the Mechanics and Physics of Solids*, **52**, 2869-2908

12. Kleiber M., 1985, *The Finite Element Method in Nonlinear Mechanics Continuum*, PWN, Warsaw [in Polish]

13. Lokander M., Reitberger T., Stenberg B., 2004, Oxidation of natural rubber-based magnetorheological elastomers, *Polymer Edgradation and Stability*, **86**, 467-471

14. Lokander M., Stenberg B., 2003a, Improving the magnetorheological effect in isotropic magnetorheological rubber materials, *Polymer Testing*, **22**, 677-680

15. Lokander M., Stenberg B., 2003b, Performance of isotropic magnetorheological rubber materials, *Polymer Testing*, **22**, 245-251

16. Matsui H., Okuda H., 1998, Treatment of the magnetic field for geodynamo simulations using the finite element method, *Earth, Planets and Space*, Tokyo

17. TOMCZYK B., KOTERAS D., 2008, Influence of air gap between coils on the magnetic field and the transformer with amorphous modular core, *Prace Naukowe Instytutu Maszyn, Napędów i Pomiarów Elektrycznych Poliechniki Wrocławskiej*, **62**, 92-97, Wrocław

18. TURNER M.J., CLOUGH R.W., MARTIN H.C., TOPP L.J., 1956, Stifness and deflection analysis of complex structures, *J. Aero. Sci.*, **23**, 805

19. DE VICENTE J., BOSSIS G., LACIS S., GUYOT M., 2002, Permability measurements in cobalt ferrite and carbonyl iron powders and suspensions, *Journal of Magnetism and Magnetic Materials*, **251**, 100-108

20. WANG D., CHEN J.-S., SUN L., 2003, Homogenization of magnetostrictive particle-filled elastomers using an interface-enriched reproducing kernel particle method, *Finite Elements in Analysis and Design*, **39**, 765-782

21. WOŹNIAK C., 1993, Nonlinear macro-elastodynamics of microperiodic composites, *Bull. Ac. Pol. Sci.: Tech. Sci.*, **41**, 315-321

22. WOŹNIAK C., 1995, Microdynamics: continuum. Modelling the simple composite materials, *J. Theor. Appl. Meeh.*, **33**, 267-289

23. YIN H.M., SUN L.Z., CHEN J.S., 2002, Micromechanics-based hyperelastic constitutive modeling of magnetostrictive particle-filled elastomers, *Mechanics of Materials*, **34**, 505-516

24. ZHOU G.Y., 2003, Shear properties of magnetorheological elastomer, *Smart Materials and Structures*, **12**, 139-146

25. ZIENKIEWICZ O.C., TAYLOR R.L., 1994, *The Finite Element Method*, 4th Ed., McGraw-Hill, London

Badanie wpływu pola magnetycznego na ferromagnetyczne kule w osnowie elastomerowej

Streszczenie

W pracy przedstawiono wyniki modelowania mikrostruktury magnetoreologicznych elastomerów (MRE) z wykorzystaniem metody elementów skończonych (MES). MRE są odpowiednikami w stanie stałym cieczy magnetoreologicznych, złożonymi z cząstek żelaza karbonylkowego i miękkiej osnowy elastomerowej. Wytwarzanie MRE prowadzone jest w stałym polu magnetycznym. Pod wpływem pola cząstki ferromagnetyczne układają się w łańcuchy wzdłuż linii pola magnetycznego, tworząc strukturę kolumnową. W analizie MES mikrostruktury MRE rozpatrzono siły magnetyczne

i sprężystości oraz ich wzajemne oddziaływania pomiędzy składnikami kompozytu. Przedstawiono przestrzenne rozmieszczenie cząstek w oparciu o ich oddziaływania w polu magnetycznym. W rozważaniach wzięto pod uwagę rozkład pola magnetycznego i momenty dipolowe cząstek. W obu przypadkach pole było zamodelowane dla kołowego przewodnika prądu elektrycznego.

Manuscript received November 8, 2009; accepted for print January 12, 2010